ELSEVIER

Physica C 291 (1997) 49–58

PHYSICA C

# The critical current of the Chevrel phase superconductor lead–molybdenum–sulphur with gadolinium

D.N. Zheng [a,*], S. Ali [a], H.A. Hamid [a], C. Eastell [b], M. Goringe [b], D.P. Hampshire [a]

[a] *Department of Physics, University of Durham, South Road, Durham DH1 3LE, UK*
[b] *Department of Materials, University of Oxford, Parks Road, Oxford OX1 3PH, UK*

Received 27 May 1997; accepted 24 August 1997

**Abstract**

The critical current density $J_c$ has been measured in a series of Chevrel phase $Pb_{1-x}Gd_xMo_6S_8$ ($x = 0$, 0.1, 0.2 and 0.3) bulk samples made using a hot isostatic pressing process. Adding Gd markedly increases the critical temperature, and the upper critical field found using resistivity, susceptibility and heat capacity measurements. The grain boundaries are found to be clean when observed using TEM. However, increasing the level of Gd, causes $J_c$ and the irreversibility field $B_{irr}$ to decrease dramatically. In particular, $J_c$ becomes more field dependent as more Gd is added. The pinning force density for all samples can be described either by a Kramer relation $F_p = J_c \times B \propto b^{1/2}(1-b)^2$ or by an exponential relation $J_c = \alpha(T)\exp[-B/\beta(T)]$, over a wide field and temperature range. This indicates that one mechanism controls $J_c$ in all the samples. This study shows that adding Gadolinium improves the intrinsic properties ($T_c$, $B_{c2}(T)$) and yet simultaneously degrades the extrinsic properties ($J_c$, $B_{irr}$). It is suggested that the Gadolinium acts as an oxygen getter which improves the intrinsic properties of the grains but causes local compositional variations at the grain boundaries which reduces $J_c$. © 1997 Elsevier Science B.V.

## 1. Introduction

The very high upper critical field of the Chevrel phase material $PbMo_6S_8$ [1,2] makes it a promising candidate as conductor material for high field superconducting magnets. A great deal of effort has been directed towards the improvement of the critical current density in bulk samples, thin films and wires made of this material [3,4]. The advancement of the fabrication techniques has led to a remarkable increase in the critical current density $J_c$ of $PbMo_6S_8$ conductors in high magnetic fields. In a recent paper, $J_c$ values in the superconductor alone for short lengths of Chevrel phase wires at 4.2 K as high as $2.4 \times 10^8$ and $0.8 \times 10^8$ A · cm$^{-2}$ at 20 and 24 T, respectively, have been reported [5]. A further increase in $J_c$ by a factor of 2 to 4, particularly in long lengths of wires will ensure that these materials fulfil the essential requirements for high field applications.

It has been reported that adding the rare-earth elements Gd or Eu can increase the upper critical field $B_{c2}$ in $SnMo_6S_8$ and $PbMo_6S_8$ [6,7]. However, very little work has addressed the effect of adding rare-earth elements on $J_c$. In this study, a series of $Pb_{1-x}Gd_xMo_6S_8$ ($x = 0$, 0.1, 0.2, and 0.3) samples were fabricated using a Hot Isostatic Press operating at 2000 atm. A comprehensive series of transport,

* Corresponding author. Tel.: +44 191 374 2123; fax: +44 191 374 3749; e-mail: d.n.zheng@durham.ac.uk.


*PII* S0921-4534(97)01684-5

magnetic, heat capacity, X-ray and electron microscopy measurements have been completed on these samples. The effect on $J_c$ of adding Gd is analyzed in detail and the mechanism that determines $J_c$ discussed.

## 2. Sample fabrication

The samples used in this study were prepared using a procedure described previously [8]. In brief, ceramic samples were first fabricated using a solid state reaction process. Pure elements with nominal composition $Pb_{1-x}Gd_xMo_6S_8$ ($x = 0$, 0.1, 0.2, and 0.3) were sealed in evacuated quartz tubes and reacted at 450°C for 4 h in an Ar atmosphere. This was followed by a slow temperature ramp at 33°C · $h^{-1}$ to 650°C and held for another 8 h. The intermediate sulphides that formed were then ground for 1 h and pressed into discs. The discs were reacted again, in evacuated and sealed quartz tubes, at 1000°C for 44 h in flowing Ar gas to form the Chevrel phase. The samples were then wrapped with Mo foil, which prevents the samples from reacting with surrounding materials, and sealed under vacuum in stainless steel tubes prior to the hot isostatic pressing treatment which was carried out at 2000 bar and 800°C for 8 h. Because oxygen can degrade the superconducting properties of the Chevrel phase compounds [9], care was taken during the fabrication process to ensure that the samples were not exposed to oxygen. This was achieved by handling the samples in a glove box which maintains a controlled atmosphere such that the oxygen concentration is less than 5 ppm and the moisture level is below 10 ppm.

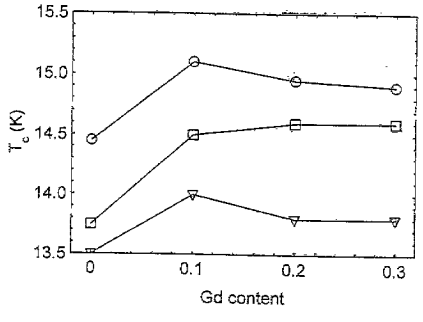


Fig. 1. The critical temperature ($T_c$) measured using heat capacity (circles), resistivity (squares) and susceptibility (triangles) for the $Pb_{1-x}Gd_xMo_6S_8$ ($x = 0$, 0.1, 0.2 and 0.3) samples.

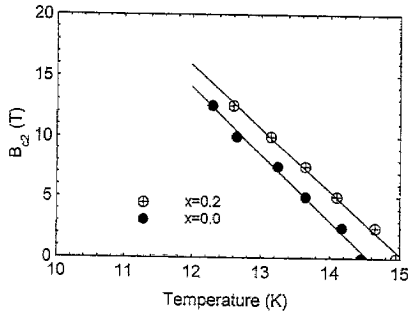


Fig. 2. The upper critical field as a function of temperature for $Pb_{1-x}Gd_xMo_6S_8$ ($x = 0$, 0.1, 0.2 and 0.3) samples measured using heat capacity.

## 3. Experimental

In Figs. 1 and 2, data of the critical temperature and the upper critical field measured using resistiv-

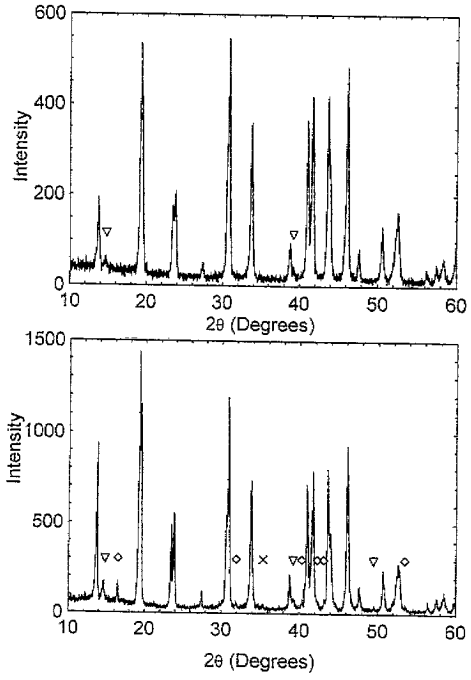


Fig. 3. The X-ray diffraction pattern of $PbMo_6S_8$ (top) and the $Pb_{0.8}Gd_{0.2}Mo_6S_8$ (bottom). The wavelength of the X-ray is 0.154 nm. The secondary phases are marked: $MoS_2$ (triangle), $Mo_2S_3$ (diamond) and $Gd_2S_3$ (cross).


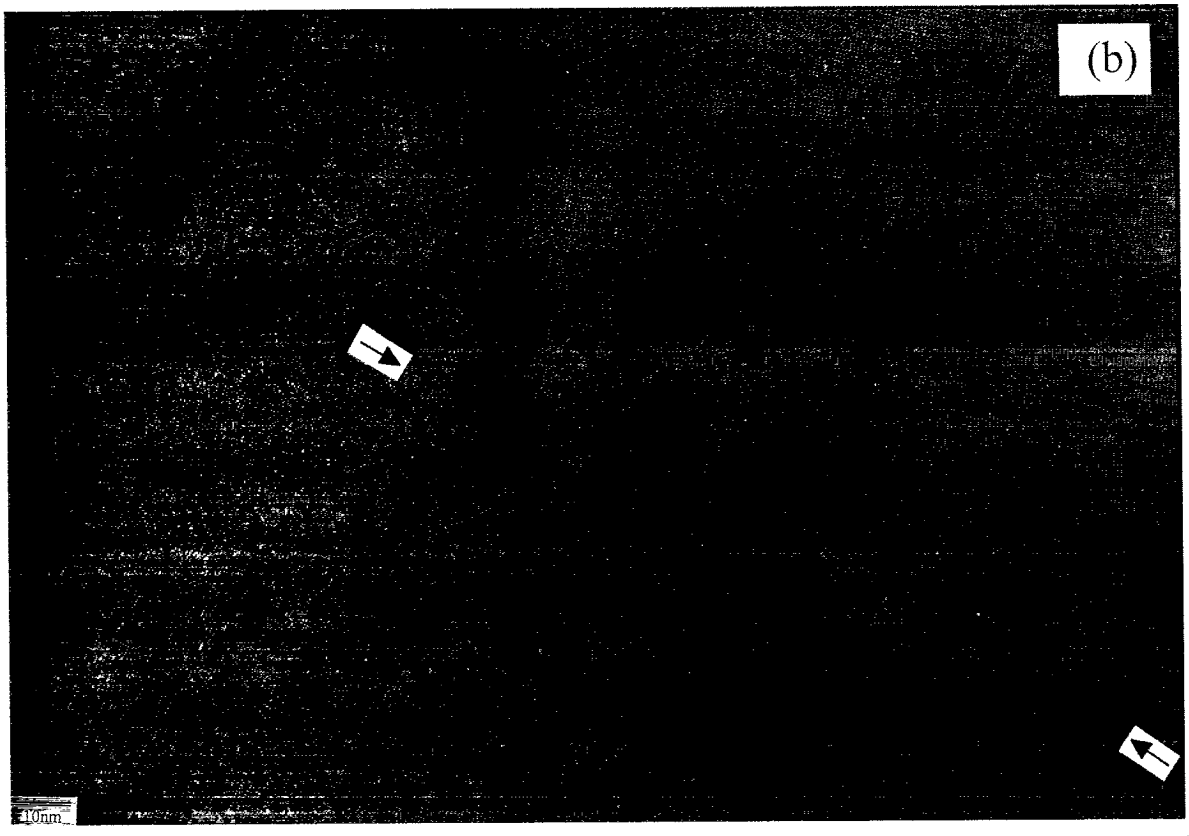


Fig. 4. TEM micrographs for $Pb_{0.7}Gd_{0.3}Mo_6S_8$ showing (a) a number of grains, (b) a lattice fringe image at grain boundaries. The grain boundary is indicated by arrows.

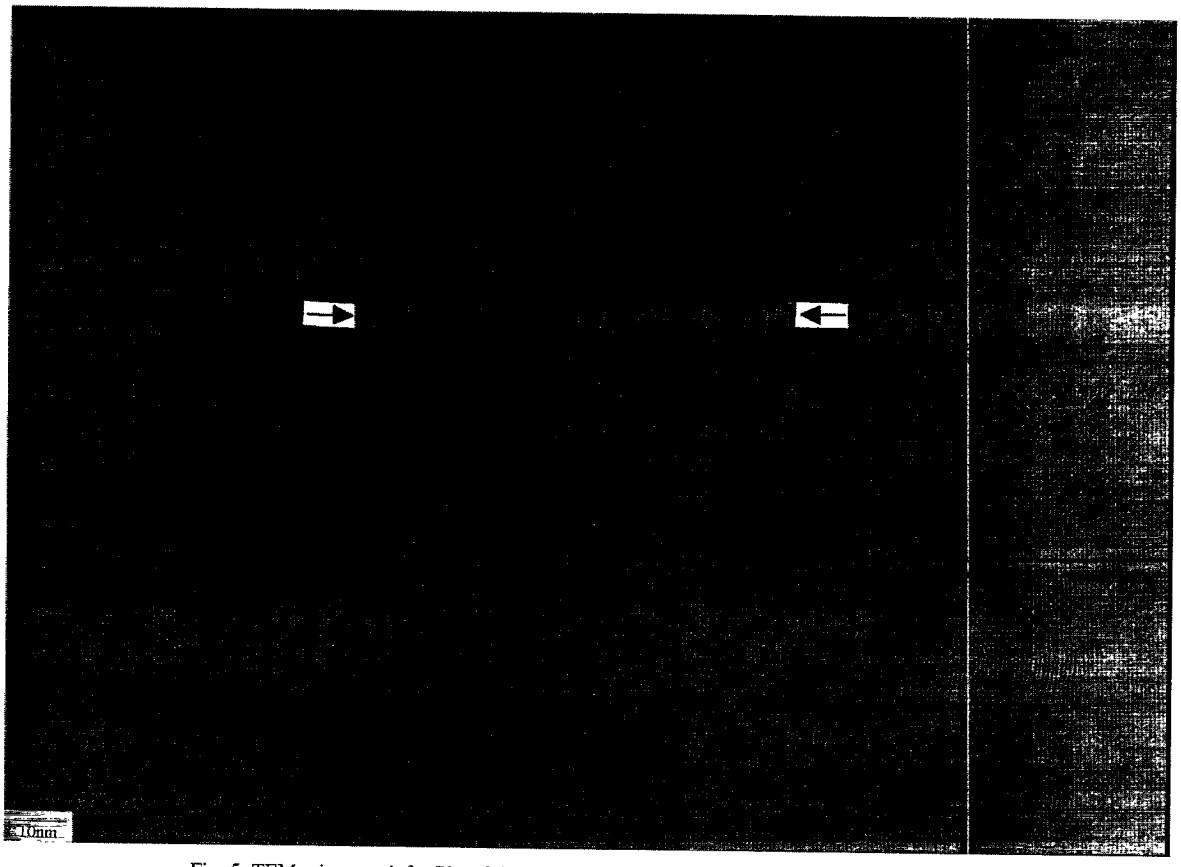


Fig. 5. TEM micrograph for $Pb_{0.8}Gd_{0.2}Mo_6S_8$ showing a planar defect indicated by arrows.

ity, susceptibility and heat capacity data are provided. The resistivity measurements were made on samples of approximate dimensions $8 \times 2 \times 2$ mm using a current of 2 mA. The susceptibility measurements were made in an AC field of 50 μT. The heat capacity measurements were made using the AC calorimetric technique [10,11]. For each measurement, the mid-point of the transition was used to define $T_c$ and $B_{c2}(T)$. The uncertainty in these critical parameters is $\pm 0.1$ K for the resistivity and susceptibility data and $\pm 0.2$ K for the heat capacity data. Figs. 1 and 2 show that by replacing 10% of the lead by Gadolinium there is initially an increase in $T_c$ by about 0.5 K and a commensurate increase in $B_{c2}(T)$ but further increases in Gd do not produce a further increase in $T_c$.

In Fig. 3, X-ray diffraction traces are shown for $PbMo_6S_8$ and $Pb_{0.8}Gd_{0.2}Mo_6S_8$. This figure shows the general trend found. With no Gadolinium, the sample is almost single phase. As the Gd content increases, the amount of the impurity phases $MoS_2$, $Mo_2S_3$ and $Gd_2S_3$ increases. However, it is clear that the majority phase in the samples is the Chevrel phase.

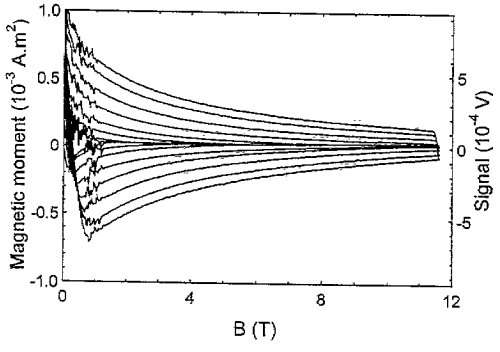


Fig. 6. Magnetic hysteresis data obtained on the $PbMo_6S_8$ sample.

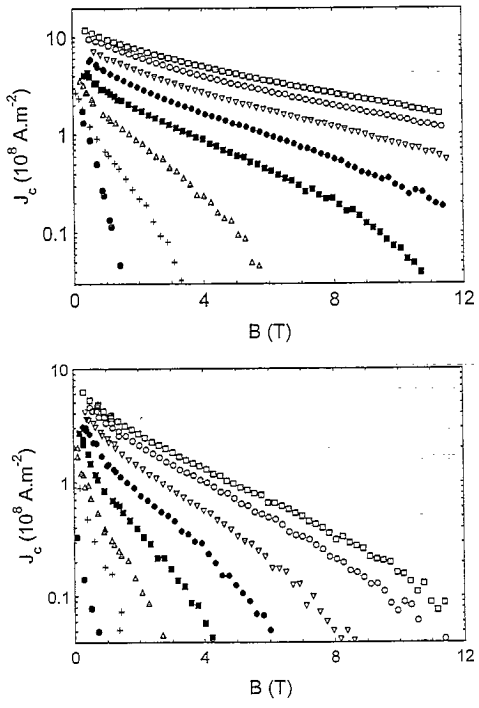


Fig. 7. Critical current density calculated using the critical state model for the $PbMo_6S_8$ (top) and the $Pb_{0.8}Gd_{0.2}Mo_6S_8$ (bottom) sample as a function of the applied field and temperature. From top to bottom: 4.2, 5, 6, 7, 8, 9, 10 and 11 K.

The TEM micrographs shown in Fig. 4 illustrate that grain boundaries between Chevrel phase grains are clean in these samples. A characteristic image of a grain boundary of $Pb_{0.7}Gd_{0.3}Mo_6S_8$ which is free of second phase is given in Fig. 4(b). Consistent with fabrication at 2000 atm, TEM shows that all the samples are more than 90% dense. Although the actual grain size ranged by a factor of 2 or 3, the average grain size for all the samples is about 0.6 $\mu$m. Furthermore, the TEM investigation revealed that the planar defects shown in Fig. 5, which have been observed in $SnMo_6S_8$ [12], are commonly seen throughout the samples.

Magnetic hysteresis curves have been measured for all the samples at temperatures from 4.2 K to $T_c$ and for fields up to 12 T. These measurements were performed with a vibrating sample magnetometer using a field sweep rate of 15 mT $\cdot$ s$^{-1}$. A typical set of data collected on the $PbMo_6S_8$ sample is given in Fig. 6. The critical current density $J_c$ is calculated from the hysteresis data using the Bean model [13]. For the rectangular shape samples used, the following formula is used:

$$J_c\,(\mathrm{A/m^2}) = \Delta M/\left[a_2(1 - a_2/3a_1)\right], \qquad (1)$$

where $\Delta M$ (A $\cdot$ m$^{-1}$) is the difference in magnetization for increasing and decreasing field, and $2a_1$ (m) and $2a_2$ (m) ($a_1 > a_2$) is the width and thickness of the sample respectively. The magnetic field dependence of $J_c$ for different temperatures is shown in Fig. 7 for the samples $PbMo_6S_8$ and $Pb_{0.8}Gd_{0.2}Mo_6S_8$. For the undoped $PbMo_6S_8$ sample the $J_c$ value at 4.2 K is slightly greater than $10^9$ A $\cdot$ m$^{-2}$ at zero field and decreases to $2 \times 10^8$ A $\cdot$ m$^{-2}$ at 10 T whereas for the $Pb_{0.8}Gd_{0.2}Mo_6S_8$ sample $J_c$ at the same temperature is reduced to $8 \times 10^8$ A $\cdot$ cm$^{-2}$ at zero field and $2 \times 10^7$ A $\cdot$ m$^{-2}$ at 10 T. Detailed complementary flux profile measurements carried out on the sample of $Pb_{0.7}Gd_{0.3}Mo_6S_8$ have also been completed. These measurements showed essentially a single slope in the flux profile, indicating that the sample is non-granular. A granular sample with weak links at grain boundaries usually shows two distinct linear parts in the flux profile [14]. These flux profile measurements confirm that the magnetic measurements in Fig. 7 characterise macroscopic intergranular critical current.

## 4. Analysis

Fig. 8 shows the Kramer plot (i.e., $J_c^{1/2}B^{1/4}$ versus $B$) for the data of $Pb_{0.8}Gd_{0.2}Mo_6S_8$ sample.

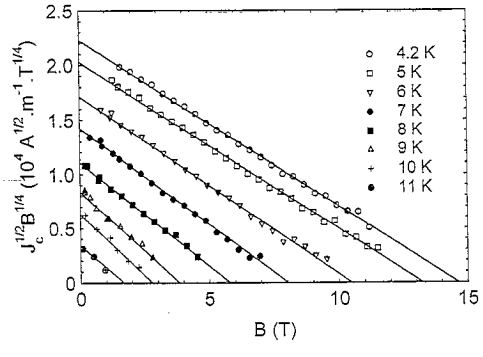


Fig. 8. A Kramer plot ($J_c^{1/2}B^{1/4}$ versus $B$) for the $Pb_{0.8}Gd_{0.2}Mo_6S_8$ sample. Linear fitting to the data is shown by solid lines.

The straight lines suggest that the pinning force $F_p$ ($= J_c \times B$) obeys the Kramer scaling formula [15],

$$F_p = \gamma B_{irr}^n b^{1/2}(1-b)^2, \quad (2)$$

where $b = B/B_{irr}$ is the normalized field and $\gamma$ is a microstructure related constant. For the other three samples, the same linear behaviour in the Kramer plot is also observed. The linear extrapolation of the data for each temperature to $J_c^{1/2}B^{1/4} = 0$ gives the irreversibility field $B_{irr}$ value at corresponding temperatures. In Fig. 9, $F_p$ is plotted after normalising $F_p$ to the peak value $F_{pmax}$ and the field by the irreversibility field $B_{irr}$. The figure shows clearly that the pinning force obeys a universal scaling relation over a wide field and temperature range which can be described by the Kramer relation. This universal scaling has been found for all the samples.

Fig. 10 gives a logarithmic plot of $F_{pmax}$ against $B_{irr}$ for the four samples. The linear fitting of the data shows that the power $n$ in Eq. (2) is approximately equal to 1.8, and $\gamma$ approximately $1.1 \times 10^7$ $A \cdot m^{-2} \cdot T^{-0.8}$.

The $B_{irr}$ values for the $Pb_{1-x}Gd_xMo_6S_8$ samples are shown in Fig. 11 and re-plotted in Fig. 12 as $\log B_{irr}$ versus $\log(1 - T/T_c)$. The data for each sample follow approximately a linear relation, suggesting that the irreversibility line for all the samples can be described by a power law relation

$$B_{irr} = B^*(1 - T/T_c)^q. \quad (3)$$

The fitting of the data give $B^* = 66$, 40, 27 and 29

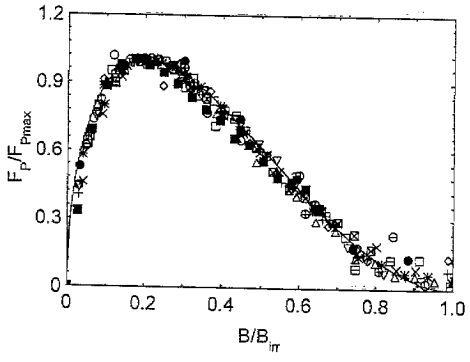


Fig. 9. Normalized plot of pinning force density $F_p$ as a function of the applied field for the samples of $Pb_{1-x}Gd_xMo_6S_8$ ($x = 0.0$, 0.1, 0.2 and 0.3). Data measured at 4.2, 6, 8, 10 K are shown. The solid line represents the normalized function proportional to $b^{1/2}(1-b)^2$.

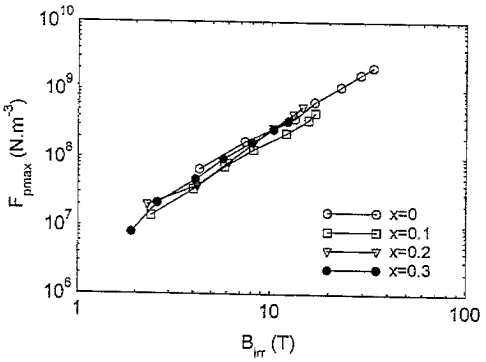


Fig. 10. Logarithmic plot of $F_{pmax}$ versus $B_{irr}$ for the $Pb_{1-x}Gd_xMo_6S_8$ ($x = 0$,0.1, 0.2 and 0.3) samples.

T for the samples with $x = 0$, 0.1, 0.2 and 0.3, respectively, while the power $q = 1.8 \pm 0.1$ for all the samples. The power law relation of the irreversibility line has been most commonly seen in high-$T_c$ superconductors. Different mechanisms have been suggested to explain the relation [16,17]. A theory of flux lattice melting [17] suggests the power $q$ should be 2 whereas a thermally activated flux flow model [16] gives $q = 1.5$. Alternatively, in conventional low temperature superconductors where $B_{irr}$ is close to $B_{c2}(T)$, $q$ is about 2 [18]. The fact that the irreversibility line of the all samples used in this study follows the same power law relation indicates that the mechanism determining the irreversibility field is similar and does not change significantly by Gd doping.

The Kramer relation can be closely approximated by an exponential magnetic field dependence for $J_c$

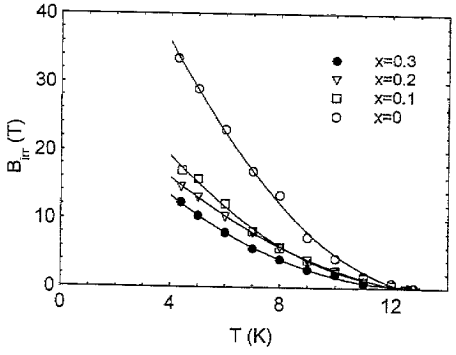


Fig. 11. Temperature dependence of the irreversibility field $B_{irr}$ data for the $Pb_{1-x}Gd_xMo_6S_8$ ($x = 0$,0.1, 0.2 and 0.3) samples. The solid lines are guides for the eye.

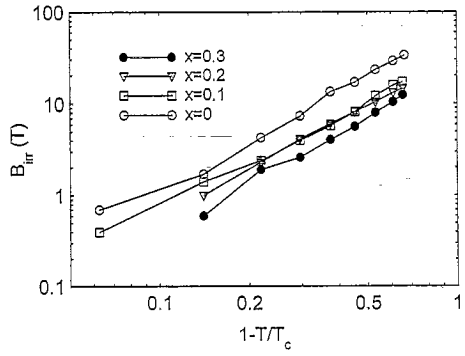


Fig. 12. Logarithmic plot of $B_{irr}$ versus $1-T/T_c$ for the $Pb_{1-x}Gd_xMo_6S_8$ ($x=0,0.1,0.2$ and 0.3) samples. The linear behaviour of the experimental data indicates a power law relation $B_{irr} \propto (1-T/T_c)^{\alpha}$.

[19]. Fig. 7 demonstrates that $J_c(B)$ can be approximated by the exponential dependence over a wide field range of the form,

$$J_c(B,T) = \alpha(T)\exp[-B/\beta(T)], \qquad (4)$$

where $\alpha(T)$ and $\beta(T)$ are functions of temperature

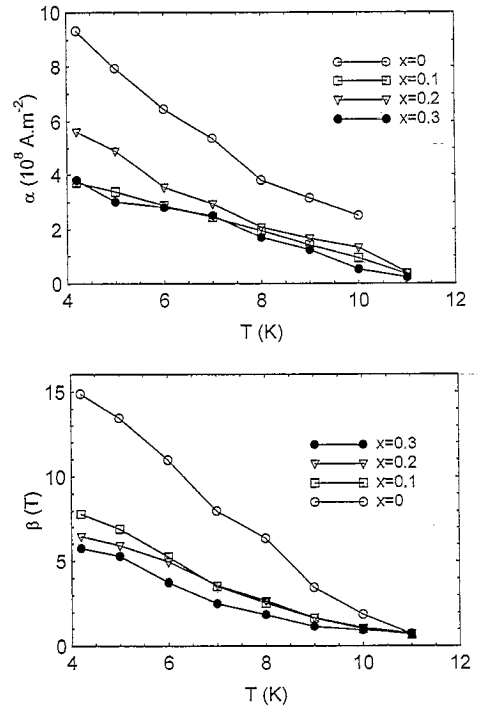


Fig. 13. Temperature dependence of parameters $\alpha$ (top) and $\beta$ (bottom) used in exponential expression Eq. (4) for the $Pb_{1-x}Gd_xMo_6S_8$ ($x=0,0.1,0.2$ and 0.3) samples.

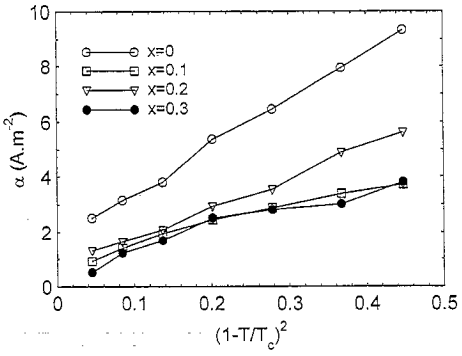


Fig. 14. Parameter $\alpha(T)$ versus $(1-T/T_c)^2$. The data are the same as those shown in the top graph of Fig. 13.

alone. By fitting the data to Eq. (4), values of $\alpha(T)$ and $\beta(T)$ can be obtained and are shown in Fig. 13 for the $Pb_{1-x}Gd_xMo_6S_8$ ($x=0,0.1,0.2$ and 0.3) samples.

The exponential magnetic field dependence of $J_c$ has been suggested by Le Lay et al. [20] as an evidence of pair-breaking through S–N–S junctions. According to the phenomenological pair-breaking S–N–S model [21], $\alpha(T)$ is proportional to $(1-T/T_c)^2$ and $\beta(T)$ is inversely proportional to the electron scattering length in the normal barrier and the width of the barrier as given by the equation

$$\beta(T) = \hbar/(2\sqrt{3}\,e\ell d), \qquad (5)$$

where $e$ is the electron charge, $\ell$ is the mean-free-path in the normal barrier, and $d$ is the width of the barrier. The exponential dependence is attributed to quantum mechanical tunnelling through the grain boundaries [20]. In Fig. 14, $\alpha(T)$ is plotted against $(1-T/T_c)^2$ for the four samples. The approximately linear behaviour indicates some limited agreement with the theory which is by no means conclusive. The parameter $\beta(T)$ decreases with increasing temperature as found in the high temperature superconductors YBaCuO [22] BiSrCaCuO [23]. At first sight, this seems to be surprising since, when the temperature increases, the mean-free-path $\ell$ should decrease in a clean normal barrier, leading to an increase of $\beta$. However, it has been argued [24] that the barrier width $d$ tends to increase with increasing temperature because of the degradation of superconductivity at grain boundaries. Therefore, the decrease of $\beta(T)$ might be explained in terms of the increasing barrier

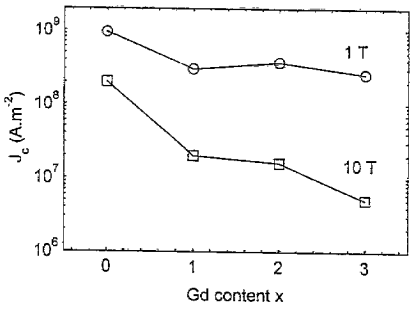


Fig. 15. Critical current density versus Gd content $x$ for the $Pb_{1-x}Gd_xMo_6S_8$ series samples. $J_c$ data were obtained at 4.2 K for two fields, 1 and 10 T, respectively.

width with increasing temperature. A very rough estimation of the magnitude of the barrier width $d$ can be found by approximating $d$ to equal to $\ell$. Using Eq. (5) and the value of $\beta$ for the $PbMo_6S_8$ sample at 4.2 K, $d$ is around 3.5 nm which is a few unit cell lengths. Figs. 13 and 14 demonstrate that increasing the Gd content decreases both $\alpha$ and $\beta$.

Fig. 15 shows the $J_c$ data at 1 and 10 T as a function of Gd content for ease of comparison with other values found in the literature. A clear feature of the data is that increasing Gd makes $J_c$ more sensitive to applied field. The current density can be extrapolated to high fields using the Kramer dependence (Eq. (2)) to find the temperature dependence of the irreversibility field (Eq. (3)). The extrapolation suggests that below 4 K, at about 30 T, there is a cross-over in $J_c$ between the bulk $PbMo_6S_8$ of this work and state-of-the-art Chevrel phase wires [5]. Below 30 T, the wires have higher $J_c$, presumably because of the small grain size produced by the $Mo_6S_8$ precursor route and the Sn doping used in fabrication. Above 30 T, the bulk material of this work has higher $J_c$ because of the higher irreversibility fields that are found.

## 5. Discussion

Universal scaling of the volume pinning force was first reported by Fietz and Webb [25]. The observation of the scaling law shown in Fig. 9, found in all the samples, suggests that only one type of mechanism controls $J_c$. This is a very striking result considering the significant difference in $J_c$ and $B_{irr}$ between the samples. Lack of scaling can occur in many systems when there are inhomogeneous materials, multiple species of pinning centres, paramagnetic limiting, matching of a flux lattice with an array of pinning centres and size effects [26]. Although the detailed physical mechanism behind the Kramer relation is still controversial [27,28], the scaling law suggests that $J_c$ is controlled by flux pinning and the elastic constants of the flux line lattice. It has been observed for different materials [8,29–31] and is useful in providing an empirical scaling law to describe $F_p$ and hence $J_c$. Kramer's relation is well established to describe $Nb_3Sn$ where grain boundaries are considered to be major pinning centres. Hence it has been suggested that grain boundaries play an important role in pinning flux lines in Chevrel phase materials [30,32]. Systematic work carried out by a number of groups has shown that $J_c$ is increased progressively when the grain size is reduced in $PbMo_6S_8$ [30,32] and $SnMo_6S_8$ [12].

Clearly, the addition of the Gd reduces the irreversibility field significantly. Within the framework of the universal scaling law, the irreversibility field can be interpreted as the effective upper critical field in the region of the pinning. Therefore, for grain boundary pinning the reduction in $B_{irr}$ is interpreted as a reduction in the critical parameters at the grain boundaries.

However, by investigating the critical current density within grains, Cattani et al. [33] have argued that in addition to the pinning at grain boundaries, there must exist strong pinning centres inside grains. The intragrain $J_c$ values they observed are more than one order of magnitude greater than the measured values of $J_c$ in the bulk. Thus, they suggest that $J_c$ of Chevrel phase bulk samples is mainly limited by the weak link nature of grain boundaries and like the high-$T_c$ superconductors, improvement of $J_c$ is expected with better connections of the grains. Additional support for the importance of intragranular pinning is provided since artificially introducing defects by neutron irradiation of $PbMo_6S_8$, increases $J_c$ [30].

The properties of the grain boundary are the primary consideration when using the pair-breaking S–N–S explanation to describe the experimental data. It suggests that the observed magnetic field dependence of $J_c$ in $PbMo_6S_8$ is determined by the weak-

link behaviour at grain boundaries. Mathematically the exponential and the Kramer relation is very similar over a wide range of the field and temperature, thus it is difficult to distinguish them experimentally [19], especially at low temperatures where the whole $F_p$ curve cannot be measured. Routes to tackle this problem include; measurements on powdered samples which consist of many individual grains but almost no grain boundaries – although additional surface pinning present in the powders but not the bulk samples can compromise this approach; measurements at very high fields, approaching the upper critical field, where it is easier to distinguish the Kramer dependence and the exponential form – although in Chevrel phase superconductors where $B_{c2}(0) \approx 60$ T, such measurements are difficult.

Although the effect of the Gadolinium on the electromagnetic transport and thermal properties has been comprehensively characterised, the reason that the Gd has had such a marked effect on improving $T_c$ and $B_{c2}(T)$ yet simultaneously degrading the $J_c$ properties is not clear. Preliminary TEM measurements show that with a few exceptions there is no Gadolinium (i.e., below the sensitivity of the instrument) either in the grains of Chevrel phase materials or in the grain boundaries between such grains. The diffusion of the Gadolinium is sufficiently slow at 1000°C and below that it remains in isolated, eventually becoming $Gd_2S_3$ grains. The isolated Gd can serve as an oxygen getter and provides a simple explanation for the improvement in the $T_c$ and $B_{c2}(T)$. Although the TEM shows that structurally, the grain boundaries are clean, the superconducting properties can change on a scale of order the coherence length which is few nanometres and the compositional variation of the grain boundaries at the nanometre scale is not known. The effect of compositional variations is extremely complex. If there were low levels of Gd at the grain boundary, the interaction between the magnetic moment of rare-earth ions and electron spins would oppose production of superconducting Cooper pairs [34]. Equally depressed levels of sulphur or lead are known to degrade the superconducting properties [35]. Detailed calculations have been completed to show the strong effect of such variations on the width of the conduction $d$-bands and the position of the Fermi level [7]. Although the detailed electronic origin for the lower $J_c$ is not known, the contrasting effect on the grains and grain boundaries remains striking.

It is well-known that the kinetics and equilibrium of grains and grain boundaries can be very different particularly in intermetallic and ceramic materials [36]. For superconductors with long coherence lengths these differences need not have a marked effect because the extended spatial averaging ensures that the properties at the grain boundaries are essentially the same as the bulk properties. In the Chevrel phase superconductors, and even more so for the high $T_c$ superconductors, the superconducting properties at the grain boundaries can be quite different to those of the bulk. An interesting feature found here is the contrast in the effect of the processing with Gadolinium on these different regions.

A large body of work on Chevrel phase materials shows that changing the grain size changes $J_c$, demonstrates flux pinning is important. Equally this work shows that materials with the same grain size and clean grain boundaries can have markedly different $J_c$. Although the theoretical framework which describes flux pinning properties at degraded grain boundaries has not yet been developed. The data generated in this work naturally leads to this type of explanation.

## 6. Summary

A series of Chevrel phase $Pb_{1-x}Gd_xMo_6S_8$ bulk samples have been made using a hot isostatic pressing process. Extensive characterisation of these samples has been completed. In the pure $PbMo_6S_8$, extrapolating the scaling law suggests that at high fields this material has $J_c$ values that are very high, characteristic of clean grain boundaries – which has been confirmed using TEM. Although the critical current and $B_{irr}$ vary markedly between the samples, the Kramer scaling law or equivalently an exponential dependence is found which suggests that the same mechanism determines $J_c$ in all the samples.

The intrinsic properties ($T_c$ and $B_{c2}$), measured using heat capacity, resistivity and susceptibility have improved by adding Gadolinium. Simultaneously, the extrinsic properties ($J_c$ and $B_{irr}$), found using magnetic data, have degraded dramatically. We suggest that the improvement in the intrinsic properties

is due to the gadolinium acting as an oxygen getter, and the degradation in the extrinsic properties is due to local compositional variations at grain boundaries. This contrast is consistent with the short coherence length of these Chevrel phase materials and exemplifies the complexity of optimising these materials for fundamental and technological studies.

## Acknowledgements

The authors wish to thank L. Le Lay (BICC Superconductors, UK) and T.C. Willis (University of Wisconsin-Madison, USA) for useful discussions; R. Luscombe for the contribution of the experimental setup. This work is supported by the Engineering and Physical Sciences Research Council UK.

## References

[1] R. Odermatt, Ø. Fischer, H. Jones, G. Bongi, J. Phys. C: Solid State Phys. 7 (1974) L13.
[2] S. Foner, E.J. McNiff Jr., E.J. Alexander, Phys. Lett. A 49 (1974) 269.
[3] B. Seeber, M. Decroux, Ø. Fischer, Phys. B 155 (1989) 129.
[4] M. Decroux, P. Selvam, J. Cors, B. Seeber, Ø. Fischer, IEEE Trans. Appl. Supercond. 3 (1993) 1502.
[5] N. Cheggour, M. Decroux, A. Gupta, Ø. Fischer, J.A.A.J. Perenboom, V. Bouquet, M. Sergent, R. Chevrel, J. Appl. Phys. 81 (1997) 6277.
[6] Ø. Fischer, M. Decroux, S. Roth, R. Chevrel, M. Sergent, J. Phys. C: Solid State Phys. 8 (1975) L474.
[7] Ø. Fischer, Appl. Phys. 16 (1978) 1.
[8] D.N. Zheng, H.D. Ramsbottom, D.P. Hampshire, Phys. Rev. B 52 (1995) 12931.
[9] S. Foner, E.J. McNiff Jr., D.G. Hinks, Phys. Rev. B 31 (1985) 6108.
[10] P.F. Sullivan, G. Seidel, Phys. Rev. 173 (1968) 679.
[11] S. Ali, Ph.D thesis, University of Durham, UK, 1996.
[12] L.A. Bonney, T.C. Willis, D.C. Larbalestier, J. Appl. Phys. 77 (1995) 6377.
[13] C.P. Bean, Rev. Mod. Phys. 36 (1964) 31.
[14] H.D. Ramsbottom, PhD thesis, University of Durham, UK, 1996.
[15] E.J. Kramer, J. Appl. Phys. 44 (1977) 1360.
[16] Y. Yeshurn, A.P. Malozemoff, Phys. Rev. Lett. 60 (1988) 2202.
[17] A. Houghton, R.A. Pelcovits, A. Subdr, Phys. Rev. B 40 (1990) 6763.
[18] M. Suenaga, A.K. Ghosh, Y.W. Xu, D.O. Welch, Phys. Rev. Lett. 66 (1991) 1777.
[19] D.P. Hampshire, in: H.C. Freyhardt (Ed.), Proc. EUCAS 1993, DGM, Germany, 1993.
[20] L. Le Lay, C.M. Friend, T. Maruyama, K. Osamura, D.P. Hampshire, J. Phys.: Condensed Matter 6 (1994) 10063.
[21] T.Y. Hsiang, D.K. Finnemore, Phys. Rev. B 22 (1980) 154.
[22] D.P. Hampshire, S.-W. Chan, J. Appl. Phys. 72 (1993) 4220.
[23] H. Yamasaki, K. Endo, S. Kosaka, M. Umeda, S. Yoshida, K. Kajimura, Phys Rev. Lett. 70 (1993) 3331.
[24] K. Osamura, S. Nonaka, M. Matsui, T. Oku, S. Ochiai, D.P. Hampshire, J. Appl. Phys. 79 (1996) 7977.
[25] W.A. Fietz, W.W. Webb, Phys. Rev. 178 (1969) 657.
[26] S.A. Alterovitz, J.A. Woollam, Phil. Mag. B 38 (1978) 619.
[27] D. Dew-Hughes, Phil. Mag. 30 (1974) 293.
[28] D.P. Hampshire, H. Jones, J. Phys. C: Solid State Phys. 21 (1987) 419.
[29] L. Le Lay, T.C. Willis, D.C. Larbalestier, Appl. Phys. Lett. 60 (1992) 775.
[30] C. Rossel, Ø. Fischer, J. Phys. F: Met. Phys. 14 (1984) 455.
[31] J.A. Woollam, S.A. Alterovitz, H.-L. Luo, in: Ø. Fischer, M.B. Maple (Eds.), Superconductivity in Ternary Compounds I, Springer-Verlag, Berlin, 1982, p. 143.
[32] V.R. Karasik, M.O. Rikel', T.G. Togonidze, V.I. Tsebro, Sov. Phys. Solid State 27 (1985) 1889.
[33] D. Cattani, J. Cors, M. Decroux, Ø. Fischer, Physica B 165 (1990) 1409.
[34] P.G. de Gennes, Superconductivity of Metals and Alloys, Addison-Wesley, 1989.
[35] H. Yamasaki, Y. Kimura, Solid State Commun. 61 (1987) 807.
[36] W.D. Kingery, H.K. Bowen, D.R. Uhlmann, Introduction to Ceramics, J. Wiley and Sons, 1960.